Invited Paper

Carrier dynamics in dilute II-VI oxide highly mismatched alloys

Yan-Cheng Lin*[a], Wu-Ching Chou[a], Jen-Inn Chyi[b], Tooru Tanaka[c]
[a]Department of Electrophysics, National Chiao Tung University, Hsinchu 30010, Taiwan
[b]Department of Electrical Engineering, National Central University, Jhongli 32001,Taiwan
[c]Department of Electrical and Electronic Engineering, Saga University, Saga 840-8502, Japan

ABSTRACT

This study explores comprehensively the carrier dynamics in ZnSeO and ZnTeO using photoluminescence (PL) and time-resolved PL spectroscopy. As the O concentration increases, the PL emissions shift toward lower energies. Additionally, the PL lifetime increases with increasing O contents and the decay curves exhibit complex behavior. In the case of ZnSeO, the mechanism of carrier recombination undergoes a complicated change from trapped to free excitons with the increase in temperature. The incorporation of O in ZnTe generates a wide distribution of electron localization below the energy of the E_- conduction subband, and these cause broad PL emission and serve as another intermediate band. Electrons in both the E_+ and the E_- conduction subbands favor rapid relaxation to low energy states. Moreover, temperature-independent long carrier lifetimes (> 130.0 ns) that are induced by localized electrons increase with O concentration.

Keywords: II-VI oxides, highly mismatched alloys, time-resolved photoluminescence, carrier dynamics, ZnSeO, ZnTeO, intermediate band

1. INTRODUCTION

An urgent and global need for renewable energy sources has engendered extraordinary research interest in potential photovoltaic materials, which aims to the gradual phasing out of conventional and nuclear power. Oxides are promising owing to their natural availability, environmental stability, and ecologically-friendly characteristics, yet traditionally limited for applications in photovoltaics by a wide band gap. Because of its large electronegativity, oxygen forms chemical bonds with almost all elements to give the corresponding oxides. Thus, band gap engineering of these highly attractive oxide materials could make them accessible for photoelectron and solar cell applications.

Dilute II-VI oxide semiconductors whose constituent anions are partially substituted by isovalent oxygen atoms of distinctly different electronegativity and size, are commonly referred to as highly mismatched alloys (HMAs).

*bryanlin@mail.nctu.edu.tw; phone +886-3-571-2121-56171; fax +886-3-572-5230

Oxide-based Materials and Devices V, edited by Ferechteh H. Teherani, David C. Look, David J. Rogers, Proc. of SPIE Vol. 8987, 89870D · © 2014 SPIE
CCC code: 0277-786X/14/$18 · doi: 10.1117/12.2039837

ZnSeO and ZnTeO are the most widely studied examples of such HMAs, exhibiting multiple band gaps and giant band gap bowing.[1-8] The unusual energy band structure of these HMAs forms according to the band anticrossing between the defect states of the substitutional minority O anions and the extended states of the host semiconductor matrix.[4,9] Since the electronegativity of the incorporated O atom is greater than those of the host Se and Te atoms, isovalent defect states form near the conduction band edge (CBE). Accordingly, the interactions that occur in ZnSeO and ZnTeO are thought to be the CB band anticrossing (CBAC). As a result the CB splits into two subbands (E_+ and E_-) with distinctly nonparabolic dispersion relations.[4,9] In ZnSeO, the O defect state is located within the CB of ZnSe, so a wide lower E_- band is formed through the anticrossing effect. However, a narrow lower band can be formed only if the defect state lies well below the CBE, and this situation occurs in ZnTeO.[4] Additionally, the strength of the anticrossing depends on the mismatch of electronegativities, which is more pronounced in ZnTeO than in ZnSeO because the mismatch between O and Te ($\Delta X = 1.4$) exceeds that between O and Se ($\Delta X = 1.1$). Therefore, in ZnTeO, the naturally formed narrow E_- band is highly separated from the higher-lying E_+ subband and acts as an intermediate band (IB), which provides additional optical transitions.

Although much research effort has focused on ZnSeO and ZnTeO, the unique decay dynamics resulted from O in these materials remains unexplored. Recently, we demonstrated that an increase in the number of isoelectronic Te localized traps complicates the carrier relaxation paths in ZnSeTe at low temperature.[10,11] In this work, we report results on the temperature-dependent photoluminescence (PL) and time-resolved PL (TRPL) of ZnSeO (O = 2.7 and 5.3 %) and ZnTeO (O = 0.43, 0.77, and 1.09 %). Complex recombination paths are clarified using the relaxation model based on various decay channels. The aim of this study is to investigate thoroughly the influence of both O and temperature on the recombination dynamics in these semiconductors, which are important for further optoelectronic applications.

2. EXPERIMENT

ZnSeO (O = 2.7 and 5.3 %) films were grown by RF-plasma assisted molecular beam exitaxy on (001) GaAs substrates following the deposition of a 100 nm-thick ZnSe buffer layer. The thicknesses of all films were fixed at around 0.5 μm. The O content was determined by x-ray diffraction (XRD) and energy-dispersive x-ray analyses. PL and TRPL were excited using a 200 ps pulsed laser diode (405 nm/10 MHz) with an excitation power of about 1 mW. An He-Cd (325 nm) laser was used to make excitation power-dependent PL measurements. Signals were dispersed using a Horiba iHR550 spectrometer with a 1800 gr/mm grating, and detected using photomultiplier tubes.

ZnTeO (O = 0.43, 0.77, and 1.09 %) films were grown by radical source molecular beam epitaxy on ZnTe (001) substrates, following a procedure that has been published previously.[7] The thickness of all films was 0.6 μm. Their O content was determined by high-resolution XRD analysis, as described elsewhere.[7] PL and TRPL were excited using 200 ps pulsed laser diodes (377 or 638 nm/2.5 MHz/1 mW). A 377 nm continuous wave laser was used to make excitation

power-dependent PL measurements. The PL and TRPL signals were dispersed using a Horiba iHR320 spectrometer with a 1200 gr/mm grating, and detected using an LN_2-cooled InGaAs photodiode and an Si photon-counting avalanche photodiode. The decay traces were recorded by time-correlated single photon counting (Time-Harp, PicoQuant).

3. RESULTS AND DISCUSSION

3.1 ZnSeO

Figure 1 (a) shows the PL spectra of ZnSeO at 10 K. Clearly, a sharp near-band-edge emission of ZnSe is observed at around 2.80 eV. When O is substituted into ZnSe, the PL emissions shift toward lower energies, which shift is accompanied by asymmetric linewidth broadening with increasing O content. The large energy redshift matches the O-induced band-gap bowing, caused by an anticrossing between the O states and the ZnSe CB states. The PL linewidth broadening is attributable to alloy fluctuations or O clustering. Excitation power-dependent PL measurements of ZnSeO (O = 2.7 %) at 10 K show a redshift of the PL peak as the laser power decreases. The PL peaks shift by about 8 meV as the laser power is decreased by three orders of magnitude. A ZnSe reference sample exhibited no change in peak position over the same decrease in power. This feature is typical of carrier localization and filling effect.

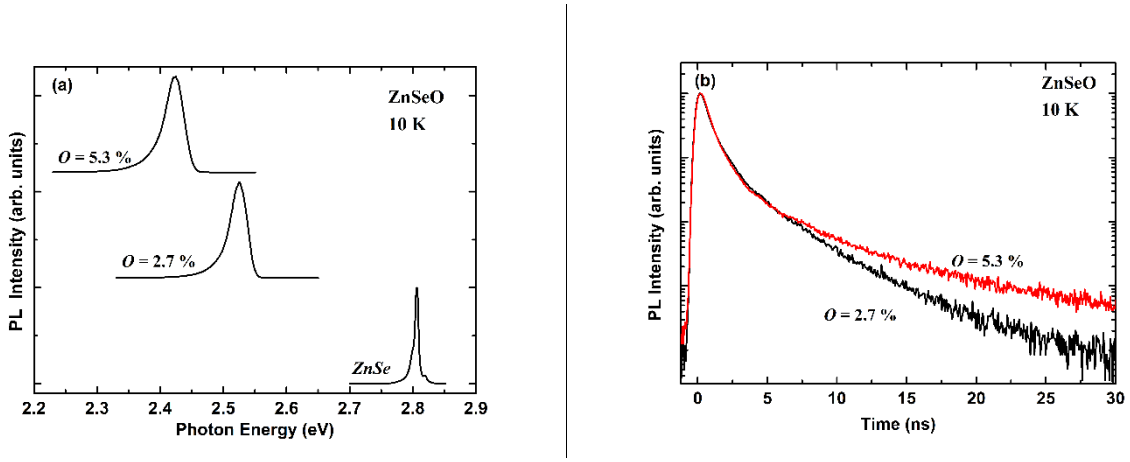

Figure 1. (a) PL and (b) TRPL spectra of ZnSe and ZnSeO at 10 K. Figure modified from [3]

Figure 1(b) shows the TRPL spectra of ZnSeO monitored at the PL peaks and 10 K. The PL decay profiles reveal nonsingle-exponential decay and can be decomposed into a fast (initial) and a slow (tail) component. The fast component is a mono-exponential decay, while the slow component is stretched-exponential decay. Obviously, the PL lifetime of the slow component significantly increases with the O concentration. The decay curves are fitted using the following equation,

$$I(t) = I_1 e^{-(t/\tau_1)} + I_2 e^{-(t/\tau_2)^{\beta}} \quad , \tag{1}$$

where β is the stretching exponent. This stretching exponent measures the relaxation rates involved in the PL decay

process, a smaller β indicates a broader rate distribution. The fitted τ_1 is around 850 ps for both samples; τ_2 (β) is around 2.8 ns (0.96) and 4.1 ns (0.93) for O = 2.7 and 5.3 %, respectively. Increasing the O concentration increases τ_2 and reduces β, implying that the slow decay originates in localized excitons (LE) due to an increasing number of trap states and decay paths. This suggestion is consistent with the hopping-transport model, in which the concentrations of the transport and trapping sites determine the β.[12]

To clarify further the dependence of the carrier dynamics in ZnSeO on temperature, temperature-dependent PL of ZnSeO (O = 5.3 %) is studied. As shown in Fig. 2(a), the PL peaks exhibit an S-shaped energy shift as the temperature is increased, which feature is typical of carrier localization. At low temperatures, a single broad band from LE dominates the PL emissions. As the temperature increases, emission from LE is rapidly thermally quenched, disappearing beyond 100 K. When the temperature is increased above 70 K, another peak appears as a higher energy shoulder of the dominant peak; it becomes more pronounced as the temperature is increased further. This emission exhibits a normal Gaussian shape (T > 120 K), while that from LE at 10 K is asymmetric, with a low-energy tail and a sharp high-energy cutoff. Moreover, this emission exhibits no obvious energy shift as the excitation power is varied by four orders of magnitude. Based on these observations, the emission at the high energy shoulder is attributed to FE, which are thermally detrapped from the isoelectronic O trap states.

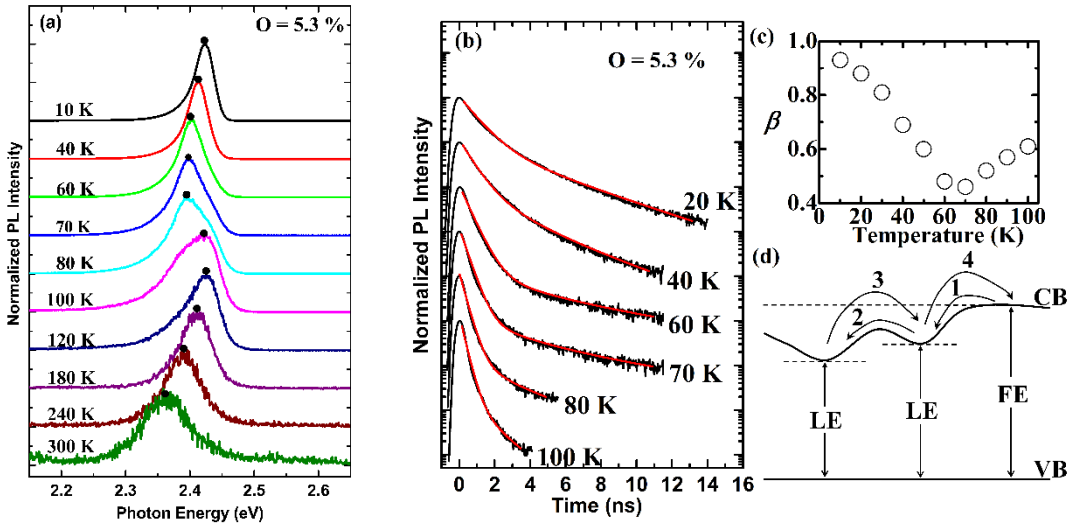

Figure 2. Temperature-dependent (a) PL and (b) TRPL spectra of ZnSeO (O = 5.3 %). (c) Stretching exponent β of ZnSeO (O = 5.3 %). (d) Schematic diagram indicates complex relaxation channels. For simplicity only two trap states are considered. Figure modified from [3]

Figure 2(b) shows the temperature-dependent TRPL spectra of ZnSeO (O = 5.3 %). Increasing the temperature significantly reduces the lifetime of the slow component. As the temperature is increased above 100 K, the slow decay component is eliminated, and the fast decay dominates the entire decay profile. Furthermore, the bending of the

logarithmic decay curve, reflecting a reduction in β, initially becomes more pronounced as the temperature increases to 70 K and then slowly diminishes, such that β begins to increase. To measure β quantitatively, the decay curves are fitted using Eq. (1). Figure 2(c) plots β against temperature. As the temperature increases, β initially decreases to a minimum at 70 K and then monotonically increases with a further increase in temperature. This phenomenon can be explained by the configuration coordinate diagram shown in Fig. 2(d). At 10 K, electrons that are generated initially in the free state hop among proximal transport and trapping sites, and recombine with O traps (channel 1). As the temperature increases, these less mobile electrons gain additional energy that enables them to hop to deeper trap states (channel 2), causing a rapid redshift in the LE peak and reducing β. Simultaneously, as the temperature approaches 70 K, some of the trapped electrons are thermally activated to repopulate the higher energy states (channel 3), leading to significant PL linewidth broadening at the high energy shoulder. At still higher temperatures, an increasing number of electrons gain sufficient energy to delocalize into the free state (channel 4) and recombine, explaining the increase in β and the blueshift of the PL peaks. Above 100 K, the slow decay component disappears because FE dominates the recombination, resulting in a monotonic PL energy redshift with the temperature.

3.2 ZnTeO

Figure 3(a) shows the PL spectra of ZnTeO (O = 0.43, 0.77, and 1.09 %) at 10 K. Notably, only broad multi-peak emissions below 2.00 eV can be observed. Such broad emissions cannot be simply attributed to the direct E_--valance band (VB) transition. Additionally, as the O content increases, the PL emissions shift rapidly downward in energy. The large PL energy redshift and the lack of ZnTe near-band-edge (NBE) emission upon the incorporation of O are strong evidence of the O-induced CBAC effect in ZnTeO. Accordingly, the absence of the E_+-VB transition in ZnTeO is attributable to the fast electron relaxation from the E_+ to the E_- or lower energy states and will be discussed later. Figure 3(b) shows the excitation power-dependent PL spectra of ZnTeO (O = 1.09 %) at 10 K. The PL peaks are redshifted by ~ 100 meV and exhibited asymmetric bandwidth broadening as the laser power is reduced by two orders of magnitude. The huge PL peak energy redshift with decreasing power reveals that the density of states exhibits an exponential tail, which arises from O clustering or alloy fluctuations, indicating possible carrier localization. The electronic states that correspond to O provide a means to trap electrons from the E_+ and the E_- conduction subbands, and local regions of higher O concentration are associated with trapping states of lower energy.

Figure 3(c) shows the TRPL spectra at 10 K. Clearly, the PL lifetimes increase with the O content and are in the range of several tens to a few hundreds of nanoseconds. The PL decay traces exhibit unusual (long decay lifetimes) and complex (curved slow profile) carrier decay dynamics. To analyze the TRPL data, a four-level rate equation model, schematically depicted in Fig. 3(d), was first adopted. However, the standard analysis procedure fails to correlate well with the curved slow decay component, implying a wide and continuous distribution of O traps. Therefore, to obtain a more quantitative measure of the decay behavior, the decay curves are all fitted using equation (1). Table I summarizes the decay

coefficients that are derived from the fits to experimental data. Increasing the O concentration markedly increases τ_2 and reduces β. These phenomena are signatures of II-VI HMAs due to the increasing number of additional decay paths for electrons, implying that the slow decay originates in LE. Moreover, increasing the O content substantially reduces/increases the magnitude of the fast/slow decay component (I_1/I_2). These facts reveal that the entire PL decay profile gradually becomes a simple stretched exponential decay,

$$I(t) = I_0 e^{-(t/\tau)^{\beta}} \quad , \tag{2}$$

where the decay curve on a double logarithmic scale is a straight line, as is the case for ZnTeO (O = 1.09 %), displayed in the inset in Fig. 3(c).

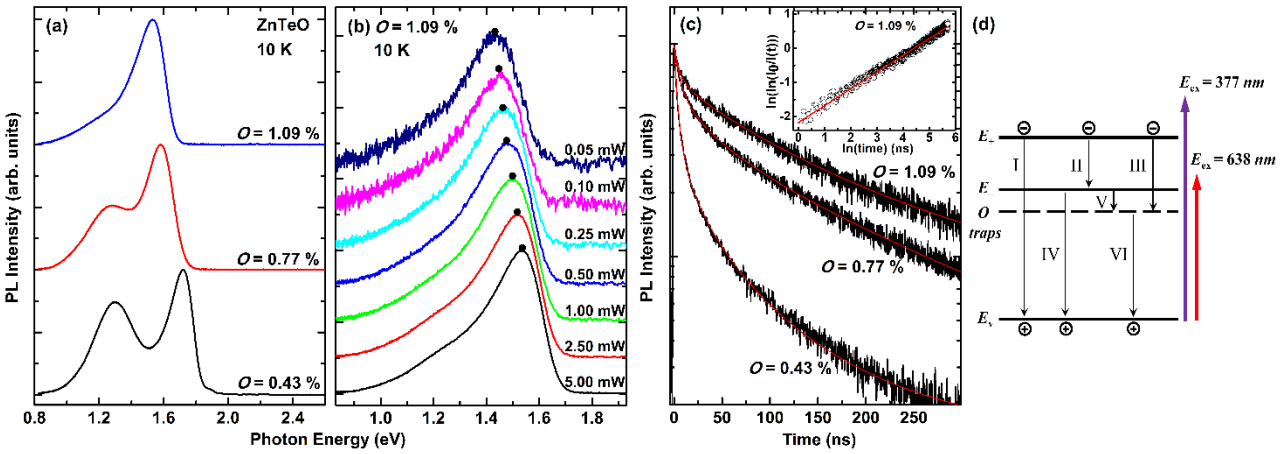

Figure 3. (a) PL (under 377 nm excitation), (b) excitation power-dependent PL, and (c) TRPL spectra of ZnTeO. Inset in (c) shows TRPL spectrum of ZnTeO (O = 1.09 %) on a double logarithmic scale. (d) Schematic energy band diagram and associated optical transitions of ZnTeO. For simplicity, only one O trapping state is considered. Figure modified from [13]

Table I. Fitting parameters of TRPL spectra in Fig. 3(c).

O Content (%)	I_1 (%)	τ_1 (ns)	I_2 (%)	τ_2 (ns)	β
0.43	60	3.6	40	29.0	0.70
0.77	20	6.0	80	106.5	0.62
1.09	5	6.3	95	134.8	0.52

Figure 3(d) shows the energy band diagram and the associated optical transitions of ZnTeO. Under 377 nm excitation, the initial fast decay of ZnTeO can be ascribed to the following effects. (i) The radiative recombination of electrons directly from the E_c to the VB [channel IV]. (ii) The radiative recombination of electrons directly from the high-energy O

traps (electrons that do not hop toward low-energy traps) to the VB [channels VI]. The nonradiative recombination is negligible since the PL is dominated by the radiative recombination at low temperature. The direct E_--VB transition could occur only in ZnTeO (O = 0.43 %) because its PL emission at high energy shoulder is close to the transition edge.

To verify this claim, Fig. 4(a) shows the TRPL spectra of ZnTeO (O = 0.43 %) at various monitored energies. Obviously, the decay time from the slow component sharply falls as the monitored energy increases, while that from the fast component is insensitive to energy. The values of τ_1, τ_2, and β are 1.7/5.8 ns, 10.4/83.5 ns, and 0.72/0.52, respectively, at 1.83/1.28 eV. This behavior implies that the electrons transfer from shallow to deep O traps. Moreover, monoexponential decay dominates the overall PL decay profile at high energy, becoming even more pronounced upon the recording of the high-energy emissions. The above results confirm the contribution of the E_--VB transition in ZnTeO (O = 0.43 %), which is responsible for the huge initial rapid decay, as shown in Fig. 3(c). Hence, the recombination of electrons directly from the higher lying O traps to the VB is the main cause of the initial fast decay in ZnTeO (O = 0.77 and 1.09 %).

The TRPL spectra of ZnTeO (O = 0.77 %) at 10 K under 377 and 638 nm excitation, shown in Fig. 4(b), further confirm the aforementioned fast carrier decay. Clearly, the spectrum obtained under 638 nm excitation exhibits faster initial decay and a larger initial decay component than that obtained using the 377 nm laser. Restated, the initial fast decay is greatly suppressed under 377 nm excitation. Similar results were observed in ZnTeO (O = 0.43 and 1.09 %). These phenomena are attributable to the feeding of photo-excited electrons from the E_+ to low-energy states [channels II and III in Fig. 3(d)], which increases the carrier delay times of channels IV and VI during the first few nanoseconds following excitation. These results further verify the rapid electron relaxation from the E_+ to the E_- or lower-energy states, which is responsible for the absence of the PL emission associated with direct E_+-VB transition [channel I in Fig. 3(d)].

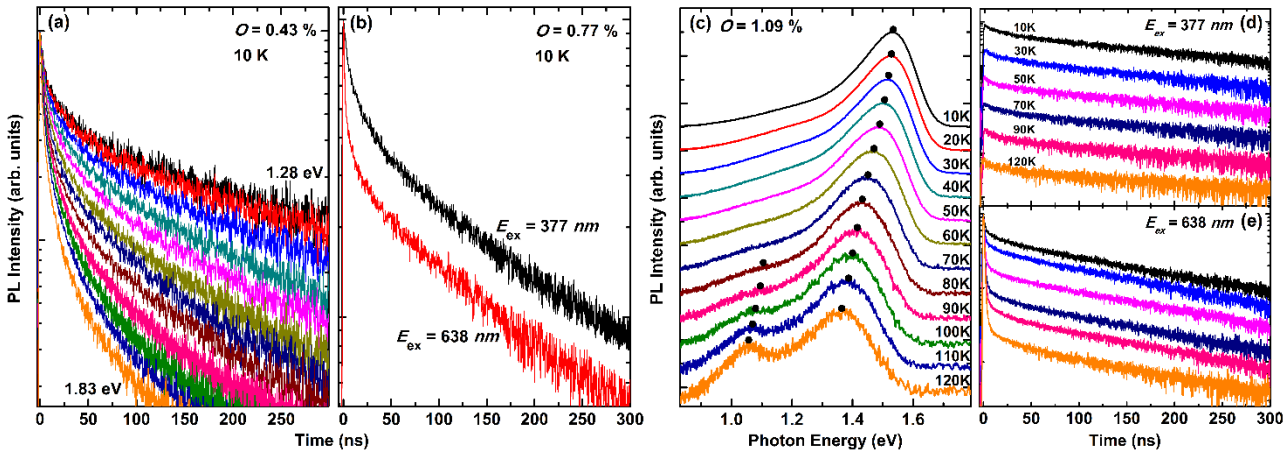

Figure 4. TRPL spectra of (a) ZnTeO (O = 0.43 %) for monitored energies from 1.83 to 1.28 eV under 377 nm excitation and (b) ZnTeO (O = 0.77 %) monitored at PL peak under 377 and 638 nm excitation. (c) Temperature-dependent PL spectra

of ZnTeO (O = 1.09 %) under 377 nm excitation and corresponding TRPL spectra obtained at PL peaks under (d) 377 nm and (e) 638 nm excitation. Figure modified from [13]

Figure 4(c) shows the temperature-dependent PL spectra of ZnTeO (O = 1.09 %) with peak positions indicated. As the temperature increases, the PL peaks shift monotonically toward lower energies; these shifts are accompanied by asymmetric bandwidth broadening. The PL peaks are redshifted by ~ 170 meV (10 -120 K), which is larger than the shift of ZnTe NBE emission (~ 120 meV; 15 - 300 K). This feature is typical of carrier localization in a variable potential that is formed by the distribution of O traps. Above 70 K, the low-energy peak suddenly appears, which demonstrates that some of the trapped electrons gain extra energy to transfer into deeper O states. Figures 4(d) and 4(e) show the temperature-dependent TRPL spectra of ZnTeO (O = 1.09 %) obtained under 377 and 638 nm excitation, respectively. Surprisingly, as revealed by Fig. 4(d), the decay curves are almost identical throughout the temperature range, except for their emission intensities. However, in Fig. 4(e), under 638 nm excitation, the initial fast decay, which is very strongly suppressed under 377 nm excitation, increasingly dominates the entire PL decay as the temperature increases. However, the slow decay remains almost unchanged. These experimental results indicate the emergence of thermally induced nonradiative recombination channels, which trigger the ultra-fast decay at high temperatures.

4. CONCLUSIONS

In summary, this study investigated the time-resolved carrier dynamics in dilute II-VI oxide, ZnSeO and ZnTeO HMAs using temperature-dependent PL and TRPL spectroscopy. In ZnSeO, the deduced stretching exponent β initially declines to a minimum as the temperature is increased to 70 K, reflecting that the recombination with the trapped electrons is significant at low temperatures. However, at higher temperatures, the free electrons that are thermally delocalized from the traps dominate the recombination. Thus, the recombination with LE gradually disappears, subsequently increasing β. In ZnTeO, The incorporation of O generates a wide distribution of electron localization below the energy of the E_- conduction subband, and these cause broad PL emission and serve as another IB. Decay curves that are induced by O traps exhibit nonsingle yet stretched exponential decay, and the corresponding temperature-independent long radiative lifetime (~ 135.0 ns for O = 1.09 %) increases with O concentration. However, electrons in both the E_+ and the E_- bands favor rapid relaxation to low energy states due to the intrinsic p-type behavior of ZnTeO and the emergence of O traps.

ACKNOWLEDGEMENT

This work was supported by the Ministry of Education and the National Science Council under Grant No. NSC 102-2112-M-009-001-MY2.

REFERENCES

[1] Shan, W., *et al.*, "Effect of oxygen on the electronic band structure in ZnO_xSe_{1-x} alloys," Appl. Phys. Lett. 83, 299 (2003).

[2] Broesler, R., *et al.*, "Temperature dependence of the band gap of $ZnSe_{1-x}O_x$," Appl. Phys. Lett. 95, 151907 (2009).

[3] Lin, Y. C., *et al.*, "Carrier dynamics in isoelectronic $ZnSe_{1-x}O_x$ semiconductors," Appl. Phys. Lett. 97, 041909 (2010).

[4] Yu, K. M., *et al.*, "Diluted II-VI oxide semiconductors with multiple band gaps," Phys. Rev. Lett. 91, 246403 (2003).

[5] Wang, W., *et al.*, "Intermediate-band photovoltaic solar cell based on ZnTe:O," Appl. Phys. Lett. 95, 011103 (2009).

[6] Tanaka, T., *et al.*, "Demonstration of $ZnTe_{1-x}O_x$ intermediate band solar cell," Jpn. J. Appl. Phys. 50, 082304 (2011).

[7] Tanaka, T., *et al.*, "Molecular beam epitaxial growth and optical properties of highly mismatched $ZnTe_{1-x}O_x$ alloys," Appl. Phys. Lett. 100, 011905 (2012).

[8] Tanaka, T., *et al.*, "Photocurrent induced by two-photon excitation in ZnTeO intermediate band solar cells," Appl. Phys. Lett. 102, 052111 (2013).

[9] Shan, W., *et al.*, "Band anticrossing in GaInNAs alloys," Phys. Rev. Lett. 82, 1221 (1999).

[10] Lin, Y. C., *et al.*, "Time-resolved photoluminescence of isoelectronic traps in $ZnSe_{1-x}Te_x$ semiconductor alloys," Appl. Phys. Lett. 93, 241909 (2008).

[11] Lin, Y. C., *et al.*, "Temperature-dependent decay dynamics in highly mismatched $ZnSe_{1-x}Te_x$ alloy," Appl. Phys. Lett. 100, 071912 (2012).

[12] Sturman, B., *et al.*, "Origin of stretched exponential relaxation for hopping-transport models," Phys. Rev. Lett. 91, 176602 (2003).

[13] Lin, Y. C., et al., "Recombination dynamics and carrier lifetimes in highly mismatched ZnTeO alloys," Appl. Phys. Lett. 103, 261905 (2013).